



# A comparative study of warping and rigid body registration for the prostate and pelvic MR volumes

Baowei Fei<sup>a</sup>, Corey Kemper<sup>a</sup>, David L. Wilson<sup>a,b,\*</sup>,<sup>1</sup>

<sup>a</sup>Department of Biomedical Engineering, Case Western Reserve University, 10900 Euclid Avenue, Cleveland, OH 44106, USA

<sup>b</sup>Department of Radiology, University Hospitals of Cleveland and Case Western Reserve University, Cleveland, OH 44106, USA

Received 2 August 2002; accepted 16 October 2002

## Abstract

A three-dimensional warping registration algorithm was created and compared to rigid body registration of magnetic resonance (MR) pelvic volumes including the prostate. The rigid body registration method combines the advantages of mutual information (MI) and correlation coefficient at different resolutions. Warping registration is based upon independent optimization of many interactively placed control points (CP's) using MI and a thin plate spline transformation. More than 100 registration experiments with 17 MR volume pairs determined the quality of registration under conditions simulating potential interventional MRI-guided treatments of prostate cancer. For image pairs that stress rigid body registration (e.g. supine, the diagnostic position, and legs raised, the treatment position), both visual and numerical evaluation methods showed that warping consistently worked better than rigid body. Experiments showed that  $\approx$  180 strategically placed CP's were sufficiently expressive to capture important features of the deformation.

© 2002 Elsevier Science Ltd. All rights reserved.

**Keywords:** Image registration; Mutual information; Thin plate spline; Prostate cancer therapy; Interventional magnetic resonance imaging

## 1. Introduction

We are investigating three-dimensional (3D) image registration, particularly with regard to minimally invasive, interventional magnetic resonance imaging (iMRI) guided treatment of prostate cancer. At our institution, we currently use iMRI on a low-field open magnet system to guide radiofrequency (RF) thermal ablation of abdominal cancer [1,2], and we are investigating this method for prostate cancer treatment. A unique feature of iMRI-guided thermal ablation is that therapy can be monitored with MR either by acquiring images of the thermally induced lesion or by measuring temperature. In addition, MR imaging of the prostate is desirable because it more accurately delineates the prostate than does CT [3], which can overestimate the prostate volume [4], and ultrasound, which has a tendency to underestimate the extent of lesions [5].

Several applications in prostate cancer diagnosis, staging, and therapy require registration of MR volumes

and/or volumes from other imaging modalities. First, registration of serial examinations can be used to follow regression/progression of tumor. Second, comparison of registered MR images acquired before and immediately after RF thermal ablation can be used to determine whether a tumor is adequately treated. This is particularly helpful in instances where the edematous response to treatment can be confused with a highly perfused tumor. Third, registration of functional, biochemical images such as single photon emission computed tomography, positron emission tomography (PET), and MR spectroscopy, to anatomical MR or CT images is useful for detecting and localizing cancer [6]. Fourth, incorporating the functional, biochemical images into the iMRI paradigm should aid image-guided treatments [7]. Finally, other treatment methods such as external radiation therapy, brachytherapy [8], and surgery, are aided by registration of images from pre-, intra-, and post-therapy for treatment planning, guidance, and assessment.

A few reports describe methods for registration in the pelvis or prostate. Manual registration has been used where an operator cues on segmented vascular structures [9] or other anatomical landmarks in the pelvis [6,10–12]. Others have used automated 3D schemes that match contours of

\* Corresponding author. Tel: +1-216-368-4099; fax: +1-216-368-4969.

E-mail address: [dlw@po.cwru.edu](mailto:dlw@po.cwru.edu) (D.L. Wilson).

<sup>1</sup> <http://imaging.ebme.cwru.edu>

bones and sometimes other structures that are extracted using manual or interactive segmentation [13–15]. Manual segmentation has also been used to create surfaces for automatic registration [16,17]. All of these methods were based on rigid body registration and required either segmentation or visual identification of structures.

We recently reported a rigid body transformation method for prostate registration [18]. For volume pairs acquired over a short time span from a supine subject with legs flat on the table, registration accuracy of both prostate centroids (typically <1 mm) and bony landmarks (average 1.6 mm) was on the order of a voxel ( $\approx 1.4$  mm). We obtained somewhat larger prostate registration errors of about 3.0 mm when volume pairs were obtained under very different conditions, e.g. legs flat and legs raised, or with and without bladder or rectal filling. Rigid body registration of the pelvis cannot follow prostate movements due to changes in the postures of legs and deformation of the bladder and rectum, as reported by us [18] and others [19,20]. In this report, we investigate the ability of warping registration to express this deformation.

Warping registration studies are reported for the brain [21,22], for the breast [23–25], for a variety of other organs [26–29], and for excised tissue [30]. Far few reports described results of the pelvis and prostate. Bharaha et al. recently reported a method using manually segmented prostate for rigid body registration followed by finite element-based warping in the application of prostate brachytherapy [31]. Voxel based methods, particularly those based upon mutual information (MI), are robust, require no segmentation that can be prone to error, are highly accurate for brain registration [32], and are suitable for abdominal registration where there can be deformation [2]. We are investigating voxel-based warping registration for the particular application in the pelvis and prostate.

There are challenges to pelvis and prostate registration. First, pelvic regions can change shape significantly, unlike the brain to which registration has been most often applied. Different patient positions such as legs flat and raised significantly change the legs in lower portions of image volumes as well as cause movement and deformation of internal organs in the pelvis. Second, the normal prostate is a small organ that when healthy measures only about 3.8 cm in its widest dimension transversely across the base [33]. Third, the small prostate is located below a much larger bladder that can change shape and size. Fourth, the prostate might move relative to the pelvic bones due to changes in bladder and rectal filling [19,20]. The alignment of the pelvic bones, a most prominent anatomical feature in MR gray-scale images, does not necessarily mean that the prostate is aligned. Finally, efficacious application of warping registration [29,30] to interventional use requires computational efficiency.

In the present study, we perform experiments to compare warping and rigid body registration for the prostate and pelvis. By using high-resolution MR images giving

distinctive anatomic detail, we test the ability of a warping algorithm to correct anatomical variations throughout the pelvic region. We include conditions with very significant changes in posture possible in interventional applications; that is, we attempt to register image volumes from a diagnostic scan with legs flat to those from a treatment acquisition with legs raised. We qualitatively and quantitatively evaluated registration results using 17 volume pairs from three volunteers.

## 2. Registration algorithm

### 2.1. Similarity measurements

We used two similarity measures, MI and correlation coefficient (CC), in our registration. Suppose one volume  $R$  is the *reference*, and the other  $F$  is *floating*. Their MI  $MI(R, F)$  is given below [34]

$$MI(R, F) = \sum_{r,f} p_{RF}(r, f) \log \frac{p_{RF}(r, f)}{p_R(r) \cdot p_F(f)}$$

The joint probability  $p_{RF}(r, f)$  and the marginal probabilities  $p_R(r)$  of the reference image and  $p_F(f)$  of the floating image, can be estimated from the normalized joint and marginal intensity histogram, respectively. The CC  $CC(R, F)$  is given below [35].

$$CC(R, F) = \frac{\sum (R(r) - \bar{R}(r))(F(f) - \bar{F}(f))}{\sqrt{\sum (R(r) - \bar{R}(r))^2 \sum (F(f) - \bar{F}(f))^2}}$$

Here  $\bar{R}(r)$ ,  $\bar{F}(f)$  denote the average intensities of the reference and floating volumes and the summation includes all voxels within the overlap of both volumes.

### 2.2. Rigid body registration algorithm with special features

Prior to warping registration, we perform rigid body registration using a method with features that make it particularly robust for MR pelvic images. We previously reported a similar method [18]. We use two similarity measures, MI and CC. We use a multi-resolution approach. At low resolution, we resample both images at 1/4 or 1/2 number of voxels along each linear dimension, respectively. We use the CC at these resolutions because it gives fewer local maximums than MI [7,18] and because it can be calculated faster than MI. We use MI at full resolution because the peaked similarity function gives a more precise solution than CC [18]. To avoid local maximums, we restart with randomly perturbed parameters obtained from a uniform distribution about the initial transformation values at the current resolution. The algorithm restarts until the absolute CC is above an experimentally determined threshold or the maximum number of restarts is reached. Absolute CC is used for the restart test rather than MI because CC has a well-defined range between 0 and 1,

because CC provides an independent check of the MI result, and because CC has fewer problems with local and incorrect global maximums for registrations at low resolution far from the optimum value [18].

We record all important results following an optimization cycle including the CC and/or MI values, the number of restarts, and the transformation parameters. At the end of processing at a lower resolution, we always select the transformation parameters having the maximum CC value. We then scale the translation parameters appropriately and assign the new parameters to be initial values at the next higher resolution. At the highest resolution, we select the final transformation parameters to be those with the maximum MI value.

Other details follow. A simplex algorithm varies the six rigid body transformation parameters (three translations and three angles) to optimize the similarity measures [36]. We use an initial guess at the lowest resolution of all zeros because the patient is normally oriented approximately the same way from one scan to the next. We set the CC thresholds at a fixed value of 0.50, and the maximum numbers of restarts at 10, 5, and 3, from low to high-resolution, respectively.

### 2.3. Warping registration using optimized control points

Fig. 1 outlines the warping registration algorithm that includes three major steps: control point selection, control point optimization, and thin plate spline warping. The unchanging volume is the reference, and the one to be warped is floating.

The manual selection of CP's is an important step. We used *RegViz*, a program written in Interactive Data Language (IDL, Research System Inc., Boulder, CO) and created in our laboratory for visualizing and analyzing image volumes. Following rigid body registration, the aligned two volumes are displayed in two rows slice-by-slice. Images can be transverse, coronal, or sagittal slices. It is quite straightforward to find corresponding features at the pelvis, prostate, bladder, and rectum. We normally select control points (CP's) using recognizable organ features such as corners and intersections of edges because of their unique positions. Corresponding CP's in the two volumes are placed using a cursor, and sometimes they are in different image slices. The 3D coordinates are automatically stored in a file. Because of the optimization that occurs later, the correspondence can be up to 15 mm or  $\approx 10$  voxels in error. Experiences with CP selection are described in Section 4. Typically, we used 180 CP's for a volume with  $256 \times 256 \times 140$  isotropic voxels.

The next step of the warping algorithm (Fig. 1) is the CP optimization. We define a small cubic volume of interest (VOI) centered at each CP. The VOI can be 16, 32, 48 or 64 voxels on a side. As reported later, the selection of VOI size depends on the amount of warping required. A simplex optimization algorithm varies the x, y, and z transformation parameters of the floating VOI until the MI with the reference VOI is optimized. Each control point is optimized independently and the 3D coordinates of the optimal CP's are recorded.

The final major step is to warp the floating volume using the corresponding optimal CP's coordinates to establish

```

Register two volumes using rigid body registration
Create a new floating volume from rigid body registration parameters
Select  $N$  control points (CP) in the reference and new floating volumes
Record 3D coordinates of the CP's in both volumes
Initialize the size of volume of interest (VOI) centered at CP's
Bin the reference and floating volumes to 256 gray levels
FOR CP FROM 0 to  $N-1$  DO BEGIN
  Optimize mutual information (MI) between the reference and floating VOI's
  1. Transform the floating VOI using three translation parameters
  2. Interpolate to get a reformatted VOI
  3. Calculate MI between the reference and reformatted VOI's
  4. Vary the three translation parameters
  5. Repeat the above steps 1-4 until meeting function tolerance or maximum iteration number
Record the optimized CP coordinates in the floating volume
END
Calculate thin plate spline transformation using the reference and optimized CP's
Interpolate the floating volume and get a warped volume
  
```

Fig. 1. Flow chart of the warping registration algorithm. Following rigid body registration,  $N$  CP's are selected in both the reference and floating volumes. A small cubic VOI is centered on each control point. Optimization is performed by varying the x, y, and z locations of the floating VOI until the MI between corresponding voxels is maximized. Each control point is optimized independently, and then the optimized CP's are used to establish a three-dimensional thin plate spline transformation for the entire volume.

a 3D thin-plate spline (TPS) transformation [37,38]. We now briefly go through the three computing steps for the TPS transformation.

First, let  $P_1 = (x_1, y_1, z_1)$ ,  $P_2 = (x_2, y_2, z_2), \dots, P_n = (x_n, y_n, z_n)$  be  $n$  control points in the image coordinate of the reference volume. Write  $r_{ij} = |P_i - P_j|$  for the distance between point  $i$  and  $j$ . We define matrices

$$P = \begin{bmatrix} 1 & x_1 & y_1 & z_1 \\ 1 & x_2 & y_2 & z_2 \\ \dots & \dots & \dots & \dots \\ 1 & x_n & y_n & z_n \end{bmatrix}, \quad n \times 4;$$

$$K = \begin{bmatrix} 0 & r_{12} & r_{13} & \dots & r_{1n} \\ r_{21} & 0 & r_{23} & \dots & r_{2n} \\ \dots & \dots & \dots & \dots & \dots \\ r_{n1} & r_{n2} & r_{n3} & \dots & 0 \end{bmatrix}, \quad n \times n;$$

and

$$L = \begin{bmatrix} K & P \\ P^T & O \end{bmatrix}, \quad (n+4) \times (n+4);$$

where  $T$  is the matrix transpose operator and  $O$  is a  $4 \times 4$  matrix of zero.

Second, let  $Q_1 = (u_1, v_1, w_1)$ ,  $Q_2 = (u_2, v_2, w_2), \dots, Q_n = (u_n, v_n, w_n)$  be  $n$  corresponding CP's in the image coordinate of the floating volume. We get matrices

$$V = \begin{bmatrix} u_1 & u_2 & \dots & u_n \\ v_1 & v_2 & \dots & v_n \\ w_1 & w_2 & \dots & w_n \end{bmatrix}, \quad 3 \times n,$$

$$Y = (V | 0 \ 0 \ 0 \ 0)^T, \quad 3 \times (n+4),$$

and define the vector  $W = (w_1, w_2, \dots, w_n)$  and the coefficients  $\alpha_1$ ,  $\alpha_x$ ,  $\alpha_y$ , and  $\alpha_z$  by the equation

$$L^{-1}Y = (W | \alpha_1 \ \alpha_u \ \alpha_v \ \alpha_w)^T.$$

Third, use the elements of  $L^{-1}Y$  to define a function  $f(u', v', w')$  everywhere in the entire volume

$$f(u', v', w') = \alpha_1 + \alpha_u u' + \alpha_v v' + \alpha_w w' + \sum_{i=0}^n w_i |P_i - (u, v, w)|.$$

Thus any voxel  $(u_i, v_i, w_i)$  in the floating volume is transformed to a new coordinate  $(u'_i, v'_i, w'_i)$  and a warped volume can be obtained by trilinear interpolation.

Additional algorithm details are now described. For both VOI optimization and rigid body registration, we use trilinear interpolation. Optimization of similarity ends either when the maximum number of calculations is reached (typically 500) or the fractional change in the similarity function is smaller than a tolerance (typically 0.001). We use IDL as the programming language.

### 3. Experimental methods

#### 3.1. Image acquisition

All MRI volumes were acquired using a 1.5 T Siemens MRI system (Magnetom Symphony, Siemens Medical Systems, Erlangen, Germany). An 8-element phased array body coil was used to ensure coverage of the prostate with a uniform sensitivity. Typically two anterior and two posterior elements were enabled for signal acquisition. We used two different MR sequences. First, a 3D FLASH sequence with TR/TE/flip parameters of 12/5.0/60 gave  $256 \times 256 \times 128$  voxels over a  $330 \times 330 \times 256 \text{ mm}^3$  field of view (FOV) to yield  $1.29 \times 1.29 \times 2.0 \text{ mm}^3$  voxels oriented to give the highest resolution for transverse slices. This sequence was good for pelvic imaging but was not ideal for prostate visualization and it was used for volunteer S1. Second, a 3D PSIF sequence with 9.4/5.0/60 (TR/TE/flip) yielded  $160 \times 256 \times 128$  voxels over a  $219 \times 350 \times 192 \text{ mm}^3$  rectangular FOV and  $1.4 \times 1.4 \times 1.5 \text{ mm}^3$  voxels oriented to give the highest resolution for transverse slices. There was over sampling at 31% in the slice direction to reduce aliasing artifacts. The second sequence gave excellent image contrast for the prostate and its surroundings and it was used for volunteers S2 and S3.

#### 3.2. Imaging experiments

We acquired 3D MRI volume images from three normal volunteers under a variety of conditions simulating anticipated conditions in diagnostic and treatment applications. Before image acquisition, each volunteer drank water and had a relatively *full bladder*. In the *diagnostic position*, the subject laid supine throughout MR scanning. In the *treatment position*, the subject was supine, and his legs were supported at 30–60° relative to the horizon and separated in a 'V' with an angle of 60–90° between two legs. This is similar to the lithotomy position used in prostate therapies, and it should provide access for needle insertion in brachytherapy or RF thermal ablation. In some experiments, the subject micturated to create an *empty bladder* prior to imaging. For each subject, image volumes were typically obtained on the same day within a 2 h session. We imaged one volunteer (S3) a week before the standard imaging session, and we refer to these volumes as *diagnosis 1 week*. Between volume acquisitions, volunteers got off the MRI table, stretched, and walked around to ensure that they would assume a different position when they laid back on the table. The coil array was centered on the prostate. All images of a volunteer were acquired with the same MRI acquisition parameters so as to ensure very similar gray values. In total, there are 4, 4, and 8 volumes for volunteer S1, S2, and S3, respectively.

The permutation of the volumes gives many possible volume pairs for registration experiments.

### 3.3. Volumes for registration experiments

We registered 17 volume pairs under five different conditions as defined above. Five pairs are *treatment–diagnosis*; seven pairs are *full bladder–empty bladder*; two pairs are *diagnosis 1 week–diagnosis*; and three pairs are *diagnosis–diagnosis*. For each case, other conditions were controlled. For example, for the case of diagnosis 1 week–diagnosis, both volumes were acquired with empty bladder and comparable conditions. Rigid body and warping registration were applied to each of the volume pairs. Results were evaluated as described next.

### 3.4. Registration evaluation

We used the multiple visualization features of RegViz to visually evaluate registration results. First, we manually segmented prostate boundaries in image slices and copied them to corresponding slices from the other volume. This enabled visual determination of the overlap of prostate boundaries over the entire volume. We applied the same method to evaluate pelvic registration. Second, color overlay displays were used to evaluate overlap of structures. One image was rendered in gray and the other in the ‘hot-iron’ color scheme available in IDL. To visualize potential differences, it was quite useful to interactively change the contribution of each image using the transparency scale. Third, we used a sector display, which divided the reference and registered images into rectangular sectors and created an output image by alternating sectors from the two input images. Even subtle shifts of edges could be clearly seen [18].

Voxel gray value measures were calculated as indicators of registration quality. MI and CC between registered volumes were computed. Since volumes to be registered were acquired using the same acquisition parameters, high absolute CC values were obtained when registration was good [24]. Because voxel intensities were comparable, we created difference images and calculated statistics such as the voxel mean and standard deviation following registration.

Finally, we used a variety of tools in RegViz to evaluate registration quality. We used contour overlap and color overlay to assess the prostate registration. We manually segmented the prostate across all slices and calculated the potential displacements of the prostate 3D centroid.

## 4. Results

### 4.1. Effect of control point selection on registration quality

In well over 100 registration experiments using different numbers and placement of CP’s, we investigated

effects on warping registration quality. For each of the three volunteers, we selected one typical volume pair from the diagnostic–treatment positions for systematic experiments. We progressively increased the number of CP’s from 15 to 250. We found that less than 120 CP’s did not produce good visual matching of our high-resolution MR images showing great anatomical detail. More than 220 CP’s did not give significant improve results but required more time for manual selection and optimization. When we used  $\approx 180$  CP’s placed strategically using rules described later, we obtained excellent results over the entire pelvis and internal organs. As a result of our experience, we modified the registration method to be suitable for many CP’s (Section 5).

Some rules follow for strategic placement of CP’s. For registration of treatment and diagnostic image volumes, most CP’s were selected using transverse slices because they best showed the pelvic displacement when moving the legs to the treatment position (Fig. 2). About 25 CP pairs were placed near edge and point features having recognizable correspondence on each of 5–8 transverse slices with a z interval of  $\approx 8$  mm, covering the entire pelvic region. Additionally, we placed about 25 CP’s from sagittal slices because they

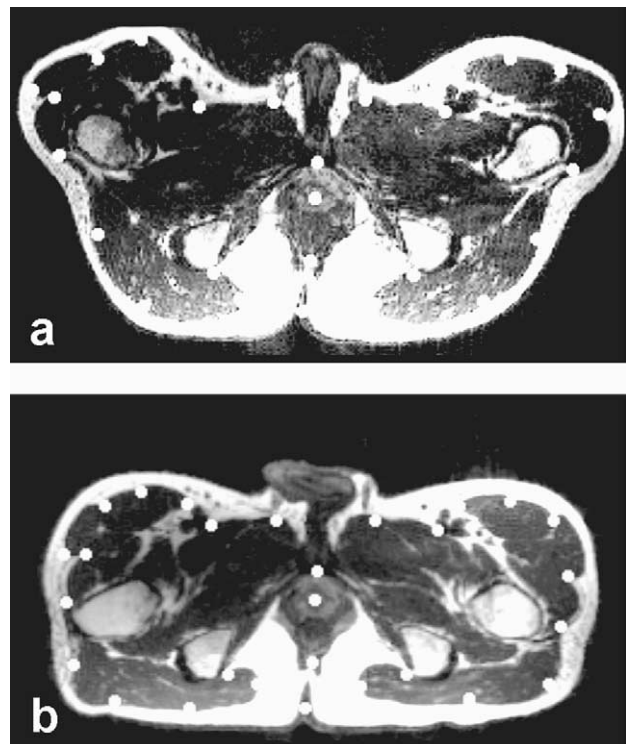


Fig. 2. Control point selection when images are acquired in the treatment and diagnostic positions. Image (a) is from the reference volume acquired in the treatment position with legs raised. Image (b) is to be warped and is from the volume acquired in the diagnostic position with the subject supine on the table. Transverse slices best show the deformations, especially at the legs. As described in the text, CP’s indicated by the white dots are selected around the pelvic surface and the prostate. Each control point is located at one voxel but displayed much bigger for better visualization. Volumes are from volunteer S2.

provided other structures that can be missed in the transverse images. It was also important to include CP's from organs other than the prostate because they constrained warps. We always placed CP's at critical regions such as the prostate center, pelvic surface, bladder border, and rectal walls.

For registration of image volumes with full and empty bladder, most CP's were placed from sagittal slices because they best showed the deformation of the bladder and rectum (Fig. 3). About 10–20 CP's were placed at the borders of the bladder and rectum on each of 8–10 sagittal slices with an equal interval of  $\approx 8$  mm, covering the entire pelvic region including the prostate, bladder, and rectum.

#### 4.2. Registration quality of warping and rigid body registration

In Fig. 4, we compare warping and rigid body registration for a typical volume pair in the treatment and diagnostic positions. Following warping registration, the prostate boundary overlap is excellent (Fig. 4(e)) and probably within the manual segmentation error. Similar results were obtained in other transverse slices throughout the prostate. The prostate 3D centroid calculated from segmented images displaced by only 0.6 mm, or 0.4 voxels, following warping. Following rigid body registration, the prostate was misaligned with a displacement to the posterior of  $\approx 3.4$  mm when in the treatment position (Fig. 4(d)), as previously reported by us [18]. Using rigid body registration, there is significant misalignment throughout large regions in the pelvis (Fig. 4(f)) that is greatly reduced with warping (Fig. 4(g)). Note that warping even allows the outer surfaces to match well. Other visualization methods such as

two-color overlays and difference images, quickly show matching of structures without segmentation but do not reproduce well on a printed page.

We next examine the effect of conditions such as bladder and rectal filling that might change from one imaging session to the next. In Fig. 5, we compare warping and rigid body registration for a volume pair with 1 week between imaging sessions. One volume is with an empty bladder and the other is with a relatively full bladder. There is also a difference in rectal filling. Warping registration closely aligns the prostate (Fig. 5(e)) while rigid body does not (Fig. 5(d)). In addition, rigid body registration does not align the bladder and parts of the rectum (Fig. 5(f)). With warping, the bladder closely matches the reference, and the rectum is better aligned (Fig. 5(g)). Other visualization methods showed excellent alignment of internal and surface edges. Difference images show that warping greatly improves alignment of internal structures as compared to rigid body registration (Fig. 6). The difference image following rigid body registration shows bright regions indicating misalignments (Fig. 6(d)) that are removed with warping (Fig. 6(e)).

We also examined volume pairs with both volumes acquired in the diagnostic position under comparable conditions. In the current data set, five volume pairs fit these criteria. In all such cases, rigid body registration worked as well as warping. There were no noticeable deformations in the pelvis, and prostate centroids typically displaced less than 1.0 mm between the two registered volumes. Note that this was obtained even though subjects always got up from the table and moved around before being imaged again.

#### 4.3. Quantitative evaluation of warping registration

Fig. 7 shows the CC and MI values between registered volumes. Warping increased CC and MI values in every case, and a paired two-tailed *t* test indicated a significant effect of warping at  $p < 0.5\%$ . The most significant improvement was in the case of treatment-diagnosis where improvements in CC and MI were as high as 102.7 and 87.8%, respectively.

Statistics of image differences following rigid body and warping registration are shown in Fig. 8. Warping reduces the absolute intensity difference between corresponding voxels (Fig. 8(a)), and the mean across all image volumes is only 4.2 gray levels, a value corresponding to only 4.7% of the mean image value of 90. We used the absolute intensity difference because signed values canceled when averaged over the entire image. The standard deviation of absolute difference is also reduced (Fig. 8(b)).

These quantitative measures match observation from visual inspection. For example, the third pair of the first group (diagnosis-treatment) in Fig. 7 and 8 corresponds the images in Fig. 4. After warping, registration greatly

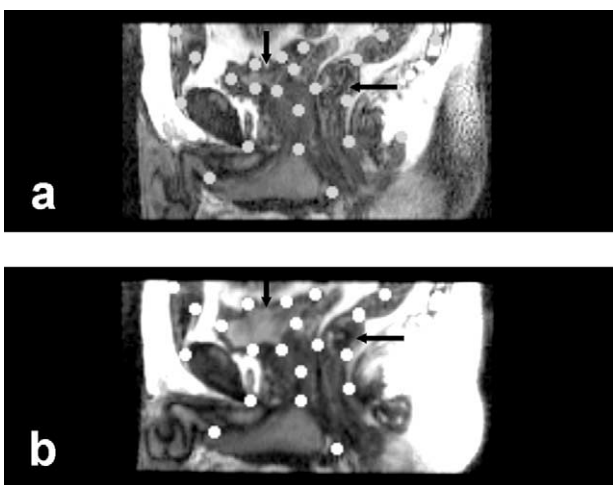


Fig. 3. Control point selection when images are acquired with a week interval between them. Image (a) is from the reference volume acquired 1 week later with an empty bladder. Image (b) is to be warped and is from the volume acquired earlier with a full bladder. Sagittal slices best show the deformations at the bladder (vertical arrow) and rectum (horizontal arrow) where most CP's are placed. Volumes are from volunteer S3.

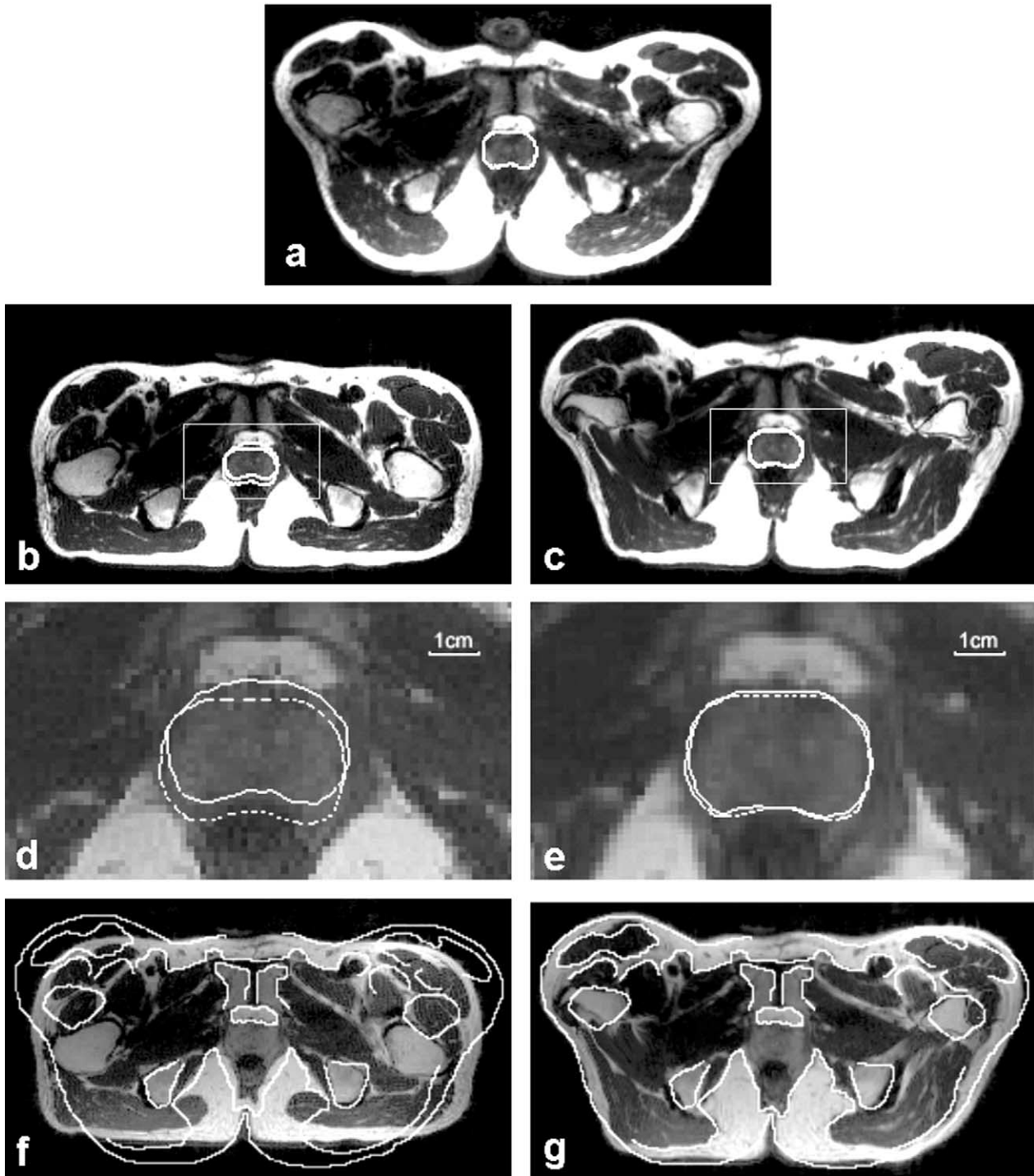


Fig. 4. Comparison of warping and rigid body registration for volumes acquired in the treatment and diagnostic positions. Image (a) is from the reference volume acquired in the treatment position, and the prostate is manually segmented. Images in the left and right columns are from the floating volume acquired in the diagnostic position following rigid body and warping registration, respectively. To show potential mismatch, the prostate contour from the reference in (a) is copied to (b) and (c) and magnified as the dashed contours in (d) and (e). The 3 mm movement of the prostate to the posterior is corrected with warping (e) but not rigid body registration (d). Pelvic boundaries manually segmented from the reference show significant misalignment with rigid body (f) that is greatly improved with warping (g). Images are transverse slices from volunteer S2.

improved. Another interesting example is the difference images in Fig. 6(d) and (e) that correspond to the last pair of the second group (full–empty bladder) in Fig. 8. Once again, the statistical measures reflect the great change in visual quality.

#### 4.4. Algorithmic implementation

In rigid body registration, the multi-resolution approach and restarting algorithm were important modifications. First, these two features improved robustness.

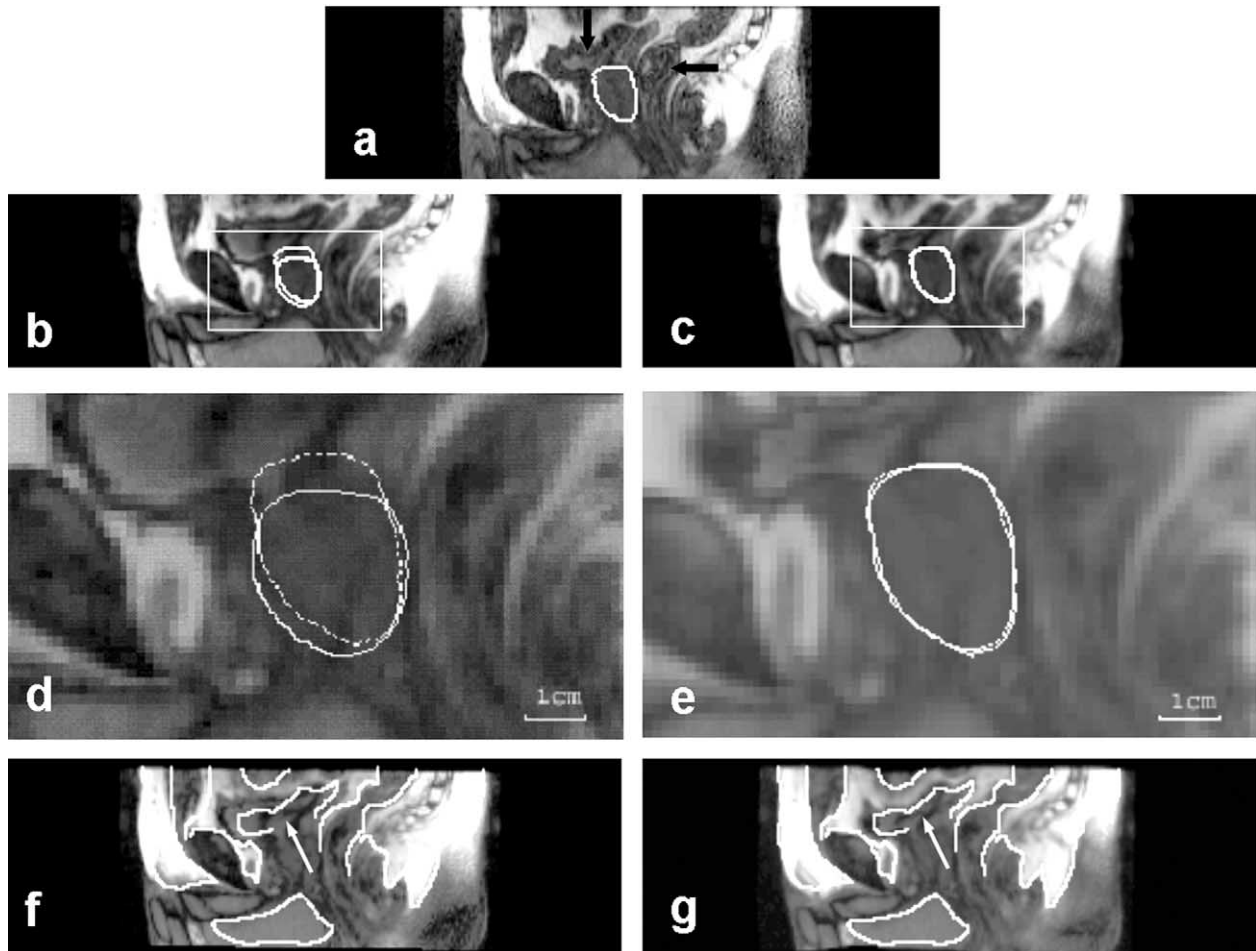


Fig. 5. Comparison of rigid body and warping registration for volumes acquired with an interval of 1 week between imaging sessions. The reference image (a) with a manually segmented prostate was acquired later with an empty bladder (vertical arrow) and partial rectal filling (horizontal arrow). Images in the left and right columns are from the floating volume acquired earlier following rigid body and warping registration, respectively. To show potential mismatch, contours from the reference are shown on images following registration, as described in Fig. 4. The full bladder in (d) has pushed the prostate, shown by the continuous curve, in the caudal direction. After warping, prostate contours match closely (e). The bladder, rectum, and other organs closely align following warping (g). With rigid body (f), proceeding from left to right, the front of the pelvis, the bladder (arrow), and the rectum are all misaligned. Images are sagittal slices from volunteer S3.

The algorithm always gave very nearly the same transformation parameters ( $<0.01$  voxels and  $0.01$  degrees) for the 17 volume pairs in this study using a wide variety of initial guesses. We also found that MI was more accurate than CC at the highest resolution [18]. Second, the multi-resolution approach enabled the program to get close to the final value quickly because of the reduced number of calculations. That is, the time for reformatting at the lowest resolution of  $1/4$  number of voxels in a linear dimension was  $0.16$  min, less than  $1/63$  times that at the highest resolution, a value nearly equal to the  $1/64$  expected from the change in the number of voxels. In a typical example, the number of restarts was 5, 1, and 1 for resolutions at  $1/4$ ,  $1/2$ , and the full number of voxels in a linear dimension, respectively. When we checked the restarts at the resolution of  $1/4$  number of voxels, we determined that none of the five restarts converged to the same transformation. It has been

our experience that more restarts are desirable at the lower resolutions, and the algorithm includes this feature. Each call to the simplex optimization resulted in 50–100 MI evaluations before the tolerance ( $0.001$ ) was reached. In some experiments on multiple volumes, we reduced the tolerance value but found little difference in registration quality, probably because of the restarting and multi-resolution features. The time for rigid body registration, typically 5–10 min on a Pentium IV, 1.8 GHz CPU, with 1.0 GB of memory, could possibly be reduced to within 1 min with optimized C code rather than the high level language IDL.

Some technical aspects of warping registration are of interest. Fig. 9 shows the optimization time and MI values between registered volumes as a function of VOI size. The optimization time for 180 CP's increases roughly linearly with the number of voxels within a VOI, about  $0.5$  min for VOI's with 16 voxels on one side and 30 min for VOI's with

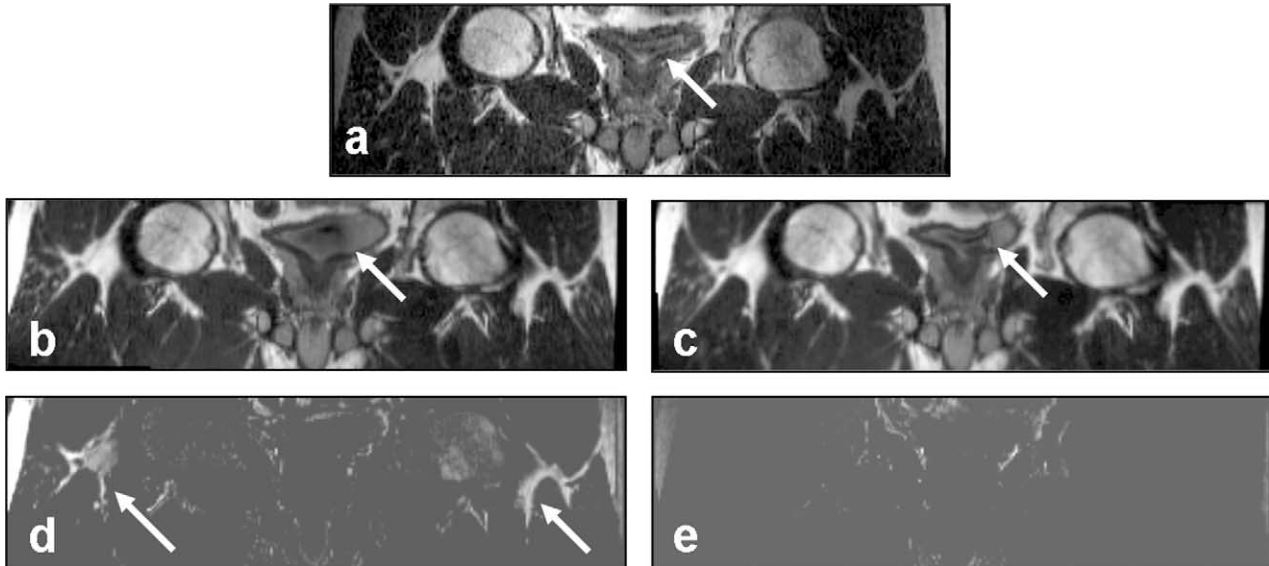


Fig. 6. Comparison of registration quality for rigid body and warping registration. The reference image (a) was acquired with a relatively empty bladder (arrow). Images (b) and (c) are from the floating volume acquired with a full bladder following rigid body and warping registration, respectively. Images (d) and (e) are the absolute difference images between the reference and registered images, respectively. Bright regions following rigid body indicate misalignments (d) that are removed with warping (e). Images (d) and (e) are displayed using the same gray-scale window and level values. Images are coronal slices from S3 volumes shown in Fig. 5.

64 voxels on a side. In Fig. 9, the MI curve saturates at the VOI size of 64 voxels on a side that means the size of 64 gave better MI value. These curves are for the case of treatment–diagnosis for volunteer S2. When we examined the cases of full–empty bladder and volumes acquired over 1 week time interval, we found that the VOI size of 16 voxels on a side worked best. Using the same computer above, for a volume with  $256 \times 256 \times 140$  voxels and 180 CP's, the warping registration typically takes about 15–45 min depending on the VOI size.

We report some details on VOI optimization for a typical treatment–diagnosis volume pair from subject S2. Following rigid body registration, the mean distance between the manually selected reference and floating CP's was  $15.5 \pm 10.7$  mm, where the latter number is the standard deviation. The maximum distance was 53.2 mm. After VOI optimization, the algorithm moved the floating CP's an average of  $9.0 \pm 6.5$  mm. This value shows that one does not have to be very careful in marking corresponding CP's.

## 5. Discussions and conclusions

### 5.1. Applicability of warping registration

For MR images of the pelvis and prostate, warping registration is desirable whenever images are acquired in different positions or with different conditions of bladder and rectal filling. Local deformations throughout the pelvis can be corrected, and, more importantly, the prostate can be accurately registered. However, when images are acquired

in the same position under comparable conditions such as our case called diagnosis–diagnosis, rigid body registration worked satisfactorily as previously reported by us [18]. Similarly, if one were to reproduce the treatment position with reasonable accuracy, we believe that prostate registration would be very good.

Our goal is to get good matching throughout the entire pelvic region not just at the prostate because proper localization of other organs is important for interpretation of some functional images and because anatomical spatial integrity is important for treatment planning. Hence, we used high-resolution MR images that provide a very stringent test for warping. Many anatomical details are evident, and even a small mismatch can clearly be seen. As a result, we found that  $\approx 180$  CP's were required to get excellent quality registration. When we applied the method to register CT images with PET images of the lung having much less resolution, many fewer points ( $\approx 50$ ) were required [39]. With a sufficient number of CP's, the TPS transformation excellently approximated the deformations of the pelvis and internal structures of our MR images. Even when we warped the volume in the diagnostic position to one in the treatment position, most organs were closely aligned, despite very significant movements. The method performed equally well for correcting the deformation and organ displacement arising from changes in bladder and rectal filling.

With our graphical user interface, interactive control point selection is quite easy after training. It usually took an experienced user about 15 min to select 180 CP's. Based on our experience, we think that it is possible to create an

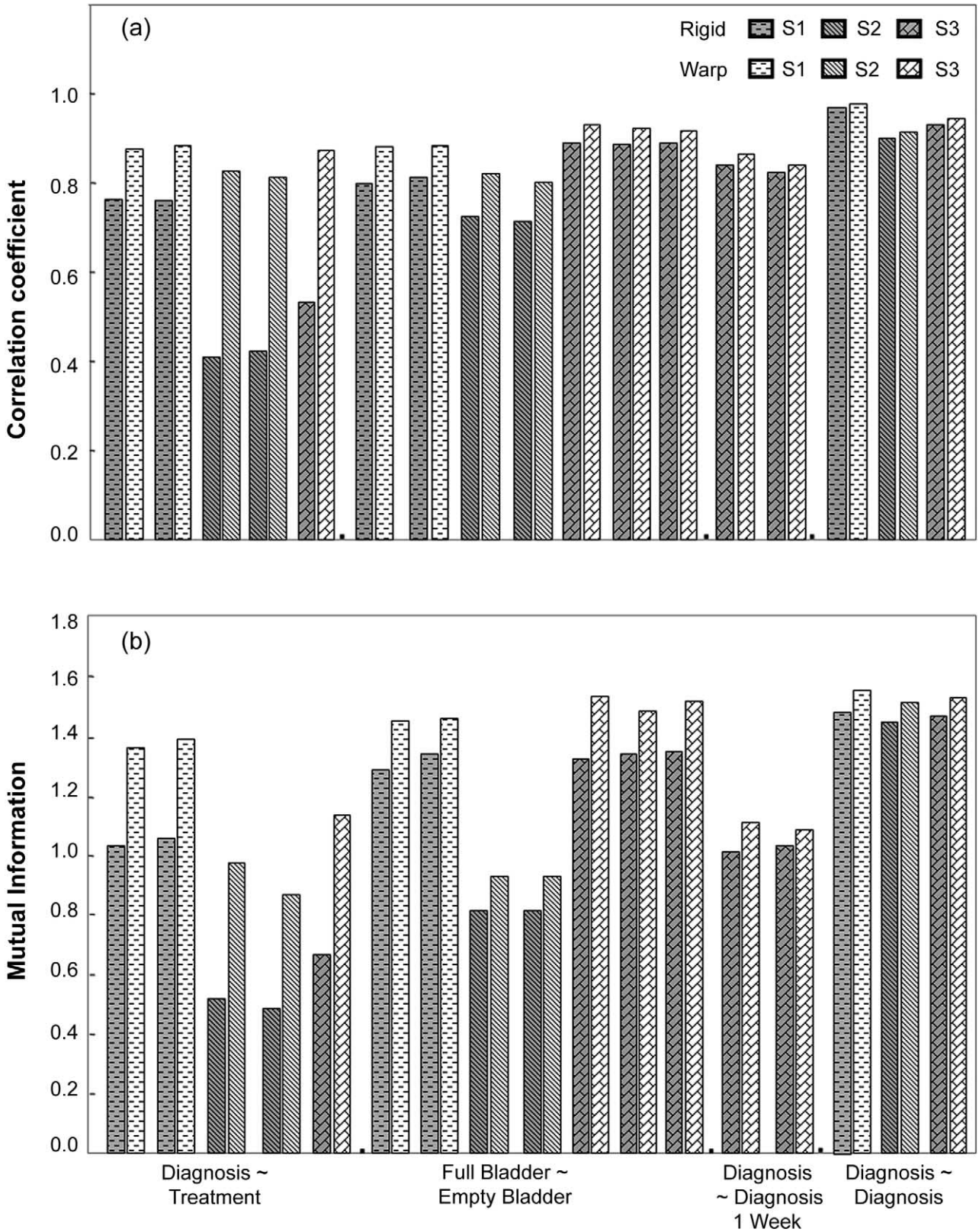


Fig. 7. Voxel similarity measures for rigid body and warping registration. CC (a) and MI (b) following registration with (light bars) and without (dark bars) warping are plotted. Conditions described in Section 3 are listed on the x-axis. Warping increased CC and MI in all cases. The most significant increases occurred in the case of the treatment-diagnosis volume pairs where maximum increases in CC and MI are 102.7% and 87.8%, respectively. For volumes acquired with in the same diagnostic position and comparable conditions (two right most groups), warping did not have significant improvement over rigid body method.

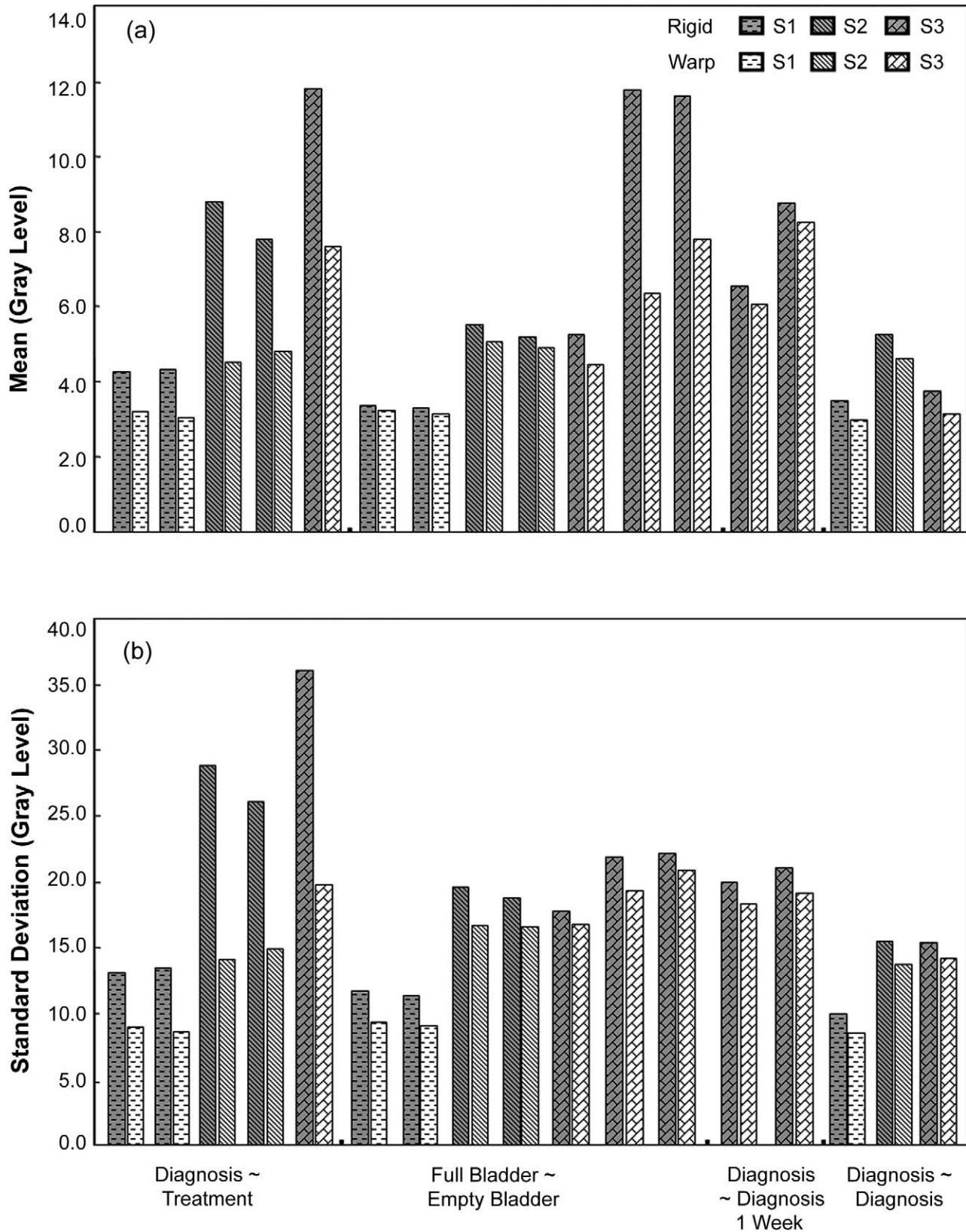


Fig. 8. Image statistics of absolute intensity difference images for rigid body and warping registration. The mean (a) and standard deviation (b) are plotted. See the legend of Fig. 7 for other details. Warping decreased the mean and standard deviation in each case, but the most significant decreases occurred in the case of the treatment-diagnosis volume pairs. After warping, the intensity averaged over all data is  $4.2 \pm 1.9$  gray levels, a value corresponding to only  $\approx 4.7\%$  of the mean image value of  $\approx 90$  gray levels.

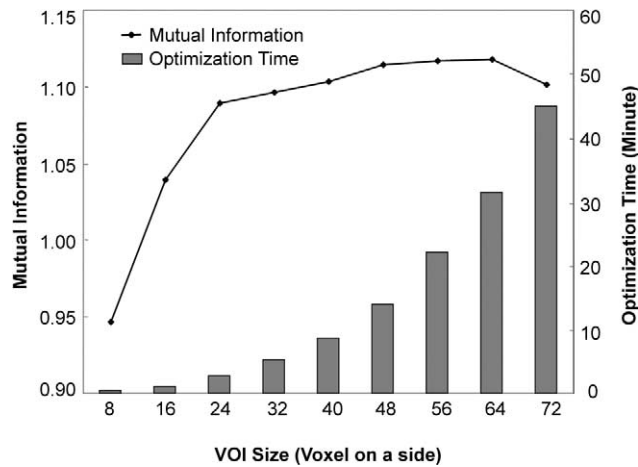


Fig. 9. Optimization time and MI as a function of VOI size. The left vertical axis is MI, and the right vertical axis is the total VOI's optimization time. The horizontal axis is the size of the VOI on a side. In each case, the VOI is centered on the CP, but since even numbers of voxels are used, the CP is displaced consistently to the upper left hand corner by one voxel. With increasing VOI size, time increases linearly with the number of voxels within the VOI. The peak MI value is at a VOI size of 64 on a side. A treatment-diagnosis volume pair is used from S2 with 180 CP's.

automatic or semiautomatic method for selection of appropriate CP's in the pelvis. For example, one might use a gray scale threshold to detect the pelvic outer boundaries and apply edge enhancement to extract feature of internal structures. CP's would be placed on such structures automatically. We are investigating this and other methods for CP selection followed by automatic warping registration.

One way to adjust the movement of CP's is to change the size of the VOI. In the case of treatment-diagnosis volume pairs, a large VOI size of 64 on a side worked better than smaller ones because displacements were large, because larger VOI's tend to give a more robust optimization, and because no small local deformations were required. However, a size of 16 on a side worked better for the case of full-empty bladder volume pairs because small VOI's better capture the small, local deformations. VOI's with a size of 64 on a side covered most of the bladder and could not generate small local deformations. For volumes with both large and small-scale deformations, we suggest using different VOI sizes for different CP's.

With warping registration, we have to be concerned about potential warping errors affecting the application of interest. For the prostate, we used 3–5 CP's near the prostate center because we desired to maintain the spatial integrity of the organ and to preserve the tissue volume. We placed many CP's around the pelvic surface to produce reasonable warping.

### 5.2. Evaluation of warping registration

Since there is no gold standard for warping registration of anatomical images, we used a variety of methods to evaluate

registration quality. First, for routine evaluation, a color overlay is simple, fast, and intuitive. To better visualize the two data sets, we interactively adjust the transparency scale of each image. Second, for illustration of subtle difference along an edge, we recommend a sector display because it best shows small shifts. Third, for visual evaluation of a specific organ such as the prostate, we like to superimpose manually marked contours from one image onto another as shown in Figs. 4 and 5. This clearly shows any displacement or deformation even in a printed figure. Fourth, a more quantitative approach is obtained by calculating the displacement in millimeters from the 3D centroid of a segmented organ such as the prostate. Finally, when images have comparable gray levels, a difference image can provide a visual evaluation or a quantitative evaluation from image statistics. A downside with MR difference images is that the inhomogeneity of the signal response and interpolation can introduce artifacts in difference images. Since MR image intensity can vary with different MR sequence parameters and the signal response of MR coil, gray value statistic may have some limitations when image acquisitions are not carefully repeated.

### 5.3. Algorithmic robustness and efficiency

The rigid body algorithm is robust for a global registration. Because of two principal design features, the algorithm is quite robust and accurate for volume pairs acquired in the same positions and with comparable conditions [18]. First, using both CC and MI at different resolutions was an important feature that increased robustness. CC gave fewer local minimums at low resolutions and MI was more accurate at high-resolution [7,18]. Second, the restarting mechanism was also quite important. Without restarting, we found that registrations sometimes failed in cases of volumes with large mismatches and significant deformation. Even these cases resulted in a proper solution when restarting was employed.

Based upon our initial experiments with interactive CP selection, we determined that many CP's were required for good matching throughout the pelvis. As a result, we designed algorithm features to be computationally efficient for TPS warping with hundreds of CP's. First, the optimization of small VOI's is very fast. Second, we optimized each CP separately because the optimization of three parameters ( $x$ ,  $y$ , and  $z$ ) is simple and fast. Conversely, as previously reported by others [26,27], the simultaneous optimization of many CP's leads to a much more complicated error surface and local maximums. If one were to use 180 CP's and optimizes the 540 free parameters simultaneously, the optimization process would become extraordinarily complex. Third, we applied the TPS transformation once to the final, optimal CP's; this saved considerable time. If TPS was applied in each iteration, the registration time would be unacceptable for our application. If we were to use optimized

C code, the total time for rigid body and warping registration should reduce to within 5 min.

#### 5.4. Applications

We discuss several points on volume interpolation. We used trilinear interpolation in the algorithm because it is fast. The final floating volume following rigid body registration is important because it is used for CP selection and warping registration. A high accurate interpolation such as sinc spline [40] can be applied to obtain this volume with reduced interpolation errors. For optimization, partial volume interpolation that was reported robust for MI-based registration [34] is another option for improvement.

The flexibility introduced with manual selection of CP's makes the current software suitable for warping registration in many applications in addition to the clinical procedures described in Section 1. We have successfully applied it to human MR–MR prostate images as shown here, rat CT–CT images, and CT–PET lung images [39]. We believe that the registration method can be applied to many organs other than the pelvis and prostate, multi-modality images, and inter-subject images. In addition, we think it applicable to a variety of animal experiments in which we are involved, including iMRI-guided thermal ablation in pig and rabbit, prostate imaging studies in dog, and controlled drug release studies in rat.

We conclude that our MI warping registration is fast and can be applied to a variety of applications. For prostate and pelvic imaging, it works better than rigid body registration whenever the subject position or condition is greatly changed between acquisitions. It will probably be a useful tool for many applications in prostate diagnosis, staging, and therapy.

## 6. Summary

Many applications in prostate cancer management such as tumor localization, possibly tumor staging, tumor targeting during therapy, assessment of adequate treatment, and treatment follow up, require image registration of MRI volumes and/or volumes from other imaging modalities. With regard to interventional MRI guided RF thermal ablation for the minimally invasive treatment of prostate cancer, registration applications include the comparison of registered MR images acquired before and immediately after RF ablation to determine whether a tumor is adequately treated. When images are acquired in different patient positions and/or different conditions, the pelvis, prostate, bladder, and rectum can deform and displace. Warping registration is desired to correct for such deformations.

We created a two-step, 3D registration algorithm using MI and thin plate spline warping for the prostate MR images. First, automatic rigid body registration was used to

capture the global transformation. Features included a multi-resolution approach, two similarity measures, and automatic restarting to avoid local minimums. Second, local warping registration was applied. Interactively placed CP's were automatically optimized by maximizing the MI of corresponding voxels in small volumes of interest and by using a three dimensional thin plate spline to express the deformation throughout the image volume. More than 100 registration experiments with 17 MR volume pairs determined the quality of registration under conditions simulating potential interventional MRI-guided treatments of prostate cancer. Evaluations included visual inspection; voxel gray value measures such as MI, CC, and intensity difference; and displacement of the centroids of segmented prostates. For image pairs that stress rigid body registration (e.g. supine, the diagnostic position, versus legs raised, the treatment position), both visual and numerical evaluation methods showed that warping consistently worked better than rigid body. Warping registration rectified the misalignment in the pelvis following rigid body registration. The prostate centroid displacement for a typical volume pair was reduced from 3.4 to 0.6 mm when warping was added. Experiments showed that  $\approx 180$  strategically placed CP's were sufficiently expressive to capture important features of the deformation. When only 120 CP's were used, warping throughout the pelvis was visually less satisfactory but the prostate was aligned reasonably well. For volume pairs with images acquired in the same position (diagnosis–diagnosis) and comparable conditions, the rigid body method worked sufficiently well, and the prostate centroid displacements were  $< 1.0$  mm. In conclusion, the warping registration method works better than rigid body registration whenever patient position or condition is greatly changed between acquisitions. It is very computational efficient for hundreds of CP's and can very well approximate the deformation of the pelvis and internal organs. It will probably be a useful tool for many applications.

## Acknowledgements

The algorithm developed in this research was supported by NIH grant R01-CA84433-01 to David L. Wilson and DOD grant DAMD17-02-1-0230 to Baowei Fei. Imaging techniques were developed under the support of NIH grant R33-CA88144-01 to Jeffrey L. Duerk.

## References

- [1] Lewin JS, Connell CF, Duerk JL, Chung YC, Clampitt ME, Spisak J, Gazelle GS, Haaga JR. Interactive MRI-guided radiofrequency interstitial thermal ablation of abdominal tumors: clinical trial for evaluation of safety and feasibility. *J Magn Resonance Imag* 1998; 8(1):40–7.
- [2] Carrillo A, Duerk JL, Lewin JS, Wilson DL. Semiautomatic 3D image registration as applied to interventional MRI liver cancer treatment. *IEEE Trans Med Imag* 2000;19(3):175–85.

- [3] Milosevic M, Voruganti S, Blend R, Alasti H, Warde P, McLean M, Catton P, Catton C, Gospodarowicz M. Magnetic resonance imaging (MRI) for localization of the prostatic apex: comparison to computed tomography (CT) and urethrography. *Radiation Oncol* 1998; 47(3):277–84.
- [4] Rasch C, Barillot I, Remeijer P, Touw A, van Herk M, Lebesque JV. Definition of the prostate in CT and MRI: a multi-observer study. *Int J Radiat Oncol Biol Phys* 1999;43(1):57–66.
- [5] Boni RAH, Boner JA, Debatin JF, Trinkler F, Kononogel H, Vonhochstetter A, Helfenstein U, Krestin GP. Optimization of prostate carcinoma staging—comparison of imaging and clinical methods. *Clin Radiol* 1995;50(9):593–600.
- [6] Sodee DB, MacLennan GT, Resnick MI, Faulhaber PF, Lee Z, Nelson AD, Molter JP, Bakale G. Comparison of CT- or MRI-fused PET-FDG and SPECT-ProstaScint (R) imaging of prostate cancer with the gold standard of histology. *J Nucl Med* 2001;42(5):1222.
- [7] Fei B, Wheaton A, Lee Z, Nagano K, Duerk JL, Wilson DL. Robust registration algorithm for interventional MRI guidance for thermal ablation of prostate cancer. Ki Mun S, editor. *Proceedings of SPIE Medical Imaging on Visualization, Display, and Image-Guided Procedures*. Bellingham WA; 2001; 4319: 53–60.
- [8] Ellis RJ, Sodee DB, Spirnak JP, Dinchman KH, O'Leary AW, Samuels MA, Resnick MI, Kinsella TJ. Feasibility and acute toxicities of radioimmunoguided prostate brachytherapy. *Int J Radiat Oncol Biol Phys* 2000;48(3):683–7.
- [9] Hamilton RJ, Blend MJ, Pelizzari CA, Milliken BD, Vijayakumar S. Using vascular structure for CT–SPECT registration in the pelvis. *J Nucl Med* 1999;40(2):347–51.
- [10] Liehn JC, Loboguerrero A, Perault X, Demange L. Superimposition of computed-tomography and single photon emission tomography immunoscintigraphic images in the pelvis-validation in patients with colorectal or ovarian carcinoma recurrence. *Eur J Nucl Med* 1992;19(3):186–94.
- [11] Balter JM, Sandler HM, Lam K, Bree RL, Lichter AS, Ten Haken RK. Measurement of prostate movement over the course of routine radiotherapy using implanted markers. *Int J Radiat Oncol Biol Phys* 1995;31(1):113–8.
- [12] Narayana V, Roberson PL, Winfield RJ, McLaughlin PW. Impact of ultrasound and computed tomography prostate volume registration on evaluation of permanent prostate implants. *Int J Radiat Oncol Biol Phys* 1997;39(2):341–6.
- [13] van Herk M, de Munck JC, Lebesque JV, Muller S, Rasch C, Touw A. Automatic registration of pelvic computed tomography data and magnetic resonance scans including a dull circle method for quantitative accuracy evaluation. *Med Phys* 1998;25(10):2054–67.
- [14] Antolak JA, Rosen II, Childress CH, Zagars GK, Pollack A. Prostate target volume variations during a course of radiotherapy. *Int J Radiat Oncol Biol Phys* 1998;42(3):661–72.
- [15] Remeijer P, Geerlof E, Ploeger L, Gilhuijs K, van Herk M, Lebesque JV. 3D portal image analysis in clinical practice: an evaluation of 2-D and 3D analysis techniques as applied to 30 prostate cancer patients. *Int J Radiat Oncol Biol Phys* 2000;46(5):1281–90.
- [16] Roeske JC, Forman JD, Mesina CF, He T, Pelizzari CA, Fontenla E, Vijayakumar S, Chen GTY. Evaluation of changes in the size and location of the prostate, seminal vesicles, bladder, and rectum during a course of external beam radiation therapy. *Int J Radiat Oncol Biol Phys* 1995;33(5):1321–9.
- [17] Scott AM, Macapinlac HA, Divgi CR, Zhang JJ, Kalaigian H, Pentlow K, Hilton S, Graham MC, Sgouros G, Pelizzari C, Chen G, Schlom J, Goldsmith SJ, Larson SM. Clinical validation of SPECT and CT/MRI image registration in radiolabeled monoclonal-antibody studies of colorectal carcinoma. *J Nucl Med* 1994; 35(12):1976–84.
- [18] Fei B, Wheaton A, Lee Z, Duerk JL, Wilson DL. Automatic MR volume registration and its evaluation for the pelvis and prostate. *Phys Med Biol* 2002;47:823–38.
- [19] vanHerik M, Bruce A, Kroes APG, Shouman T, Touw A, Lebesque JV. Quantification of organ motion during conformal radiotherapy of the prostate by three dimensional image registration. *Int J Radiat Oncol Biol Phys* 1995;33(5):1311–20.
- [20] Tenhaken RK, Forman JD, Heimburger DK, Gerhardtsson A, Mcshan DL, Pereztamayo C, Schoeppel SL, Lichter AS. Treatment planning issues related to prostate movement in response to differential filling of the rectum and bladder. *Int J Radiat Oncol Biol Phys* 1991;20(6): 1317–24.
- [21] Rohr K, Stiehl HS, Sprengel R, Buzug TM, Weese J, Kuhn MH. Landmark-based elastic registration using approximating thin-plate splines. *IEEE Trans Med Imag* 2001;20(6):526–34.
- [22] Maurer CR, Hill DLG, Martin AJ, Liu HY, McCue M, Rueckert D, Lloret D, Hall WA, Maxwell RE, Hawkes DJ, Truwit CL. Investigation of intraoperative brain deformation using a 1.5-t interventional MR system: preliminary results. *IEEE Trans Med Imag* 1998;17(5):817–25.
- [23] Davis MH, Khotanzad A, Flamig DP, Harms SE. A physics-based coordinate transformation for 3D image matching. *IEEE Trans Med Imag* 1997;16(3):317–28.
- [24] Rueckert D, Sonoda LI, Hayes C, Hill DLG, Leach MO, Hawkes DJ. Nonrigid registration using free-form deformations: application to breast MR images. *IEEE Trans Med Imag* 1999;18(8):712–21.
- [25] Denton ERE, Sonoda LI, Rueckert D, Rankin SC, Hayes C, Leach MO, Hill DLG, Hawkes DJ. Comparison and evaluation of rigid, affine, and nonrigid registration of breast MR images. *J Comp Assisted Tomography* 1999;23(5):800–5.
- [26] Meyer CR, Boes JL, Kim B, Bland PH, Zasadny KR, Kison PV, Koral K, Frey KA, Wahl RL. Demonstration of accuracy and clinical versatility of mutual information for automatic multimodality image fusion using affine and thin-plate spline warped geometric deformations. *Med Image Anal* 1996;1(3):195–206.
- [27] Krucker JF, Meyer CR, LeCarpentier GL, Fowlkes JB, Carson PL. 3D spatial compounding of ultrasound images using image-based nonrigid registration. *Ultrasound Med Biol* 2000;26(9):1475–88.
- [28] Kimiaei S, Noz M, Jonsson E, Crafoord J, Maguire GQ. Evaluation of polynomial image deformation using anatomical landmarks for matching of 3D-abdominal MR-images and for atlas construction. *IEEE Trans Nucl Sci* 1999;46(4):1110–3.
- [29] Wilson DL, Carrillo A, Zheng L, Genc A, Duerk JL, Lewin JS. Evaluation of 3D image registration as applied to MR-guided thermal treatment of liver cancer. *J Magn Resonance Imag* 1998; 8(1):77–84.
- [30] Kim B, Boes JL, Frey KA, Meyer CR. Mutual information for automated unwarping of rat brain autoradiographs. *Neuroimage* 1997; 5(1):31–40.
- [31] Bharatha A, Hirose M, Hata N, Warfield SK, Ferrant M, Zou KH. Three-dimensional finite element-based deformable registration of pre- and intraoperative prostate imaging. *Radiology* 2001;221:224.
- [32] West J, Fitzpatrick JM, Wang MY, Dawant BM, Maurer CR, Kessler RM, Maciunas RJ, Barillot C, Lemoine D, Collignon A, Maes F, Suetens P, Vandermeulen D, vandenElsen PA, Napel S, Sumanaweera TS, Harkness B, Hemler PF, Hill DLG, Hawkes DJ, Studholme C, Maintz JBA, Viergever MA, Malandain G, Pennec X, Noz ME, Maguire GQ, Pollack M, Pelizzari CA, Robb RA, Hanson D, Woods RP. Comparison and evaluation of retrospective intermodality brain image registration techniques. *J Comp Assisted Tomography* 1997; 21(4):554–66.
- [33] Gray H. *Anatomy, Descriptive and Surgical* (The classic collector's edition). New York: Gramercy Books; 1977. p. 1010.
- [34] Maes F, Collignon A, Vandermeulen D, Marchal G, Suetens P. Multimodality image registration by maximization of mutual information. *IEEE Trans Med Imag* 1997;16(2):187–98.
- [35] Press WH, Flannery BP, Teukolsky SA, Vetterling WT. *Numerical recipes in C: the art of scientific computing*, 2nd ed. New York: Cambridge University Press; 1993.

- [36] Nelder J, Mead RA. A simplex method for function minimization. *Comp J* 1965;7:308–13.
- [37] Goshtasby A. Registration of images with geometric distortions. *IEEE Trans Geosci Remote Sensing* 1988;26(1):60–4.
- [38] Bookstein FL. Thin-plate splines and the atlas problem for biomedical images. *Lecture Notes in Comp Sci* 1991;511:326–42.
- [39] Lee Z, Kemper C, Muzic RF, Berridge MS, Wilson DL. Quantitative pulmonary imaging based on PET–CT co-registration with warping. *J Nucl Med* 2001;42:10–11.
- [40] Thacker NA, Jackson A, Moriarty D, Vokurka E. Improved quality of re-sliced MR images using re-normalized sinc interpolation. *J Magn Resonance Imag* 1999;10(4):582–8.

**Baowei Fei** received his B.S. (1990) and M.S. (1995) in Biomedical Engineering from Xi'an Jiaotong University, China, where he received the Science and Technological Award from the National Department of Education in 1993. He obtained his PhD (1998) from Shanghai Jiao Tong University, China, where he was awarded the Honor of Excellent Graduate Student of the Year 1998 of Shanghai. From 1998 to 2000, he worked as a Research Fellow at the Computer Integrated Medical Intervention Laboratory of Nanyang Technological University, Singapore. He is currently a Senior Research Associate in the Department of Biomedical Engineering at Case Western Reserve University. In 2001, he won the Postdoctoral Traineeship Award from the US Department of Defense Congressionally Directed Medical Research Program. He is an active member of IEEE and SPIE. He has over 10 years of experience in biomedical engineering with research interests in biomedical image analysis and registration, interventional MRI, medical robotics and computer-aided surgery.

**Corey Kemper** received her BS in Biomedical Engineering from Case Western Reserve University (CWRU) in 2001. In the same year, she was also named CWRU's Engineering Student of the Year. Currently, she is pursuing a PhD in the Electrical Engineering and Computer Science Department at the Massachusetts Institute of Technology (MIT) on a fellowship awarded by the Whitaker Foundation. She continues to work in biomedical imaging research as part of the Medical Vision Group in the Artificial Intelligence Laboratory at MIT and in the Surgical Planning Laboratory at the Brigham and Women's Hospital.

**David L. Wilson** is currently a Professor in the Departments of Biomedical Engineering and Radiology at Case Western Reserve University (CWRU). His PhD is from Rice University. He has authored over 60 refereed journal papers and over 80 proceedings papers and book chapters, and he holds six patents in interventional medical imaging. He has served as an organizer of biomedical engineering conferences and reviewer for federal funding agencies. He has a history of substantial federal funding in biomedical imaging. He has been a leader in developing biomedical imaging research and education at CWRU including teaching core courses, advising a large number of graduate and undergraduate students, chairing faculty search committees, and co-authoring several successful developmental proposals to foundations and to state and federal agencies. His research interests include biomedical image analysis, interventional MRI, quantitative image quality, and molecular imaging.

Fei BW, Kemper C, Wilson DL. A comparative study of warping and rigid body registration for the prostate and pelvic MR volumes. *Computerized Medical Imaging and Graphics* 2003;27:267-281.

Copyright 2002 Elsevier Science Ltd. One print or electronic copy may be made for personal use only. Systematic reproduction and distribution, duplication of any material in this paper for a fee or for commercial purposes, or modification of the content of the paper are prohibited.